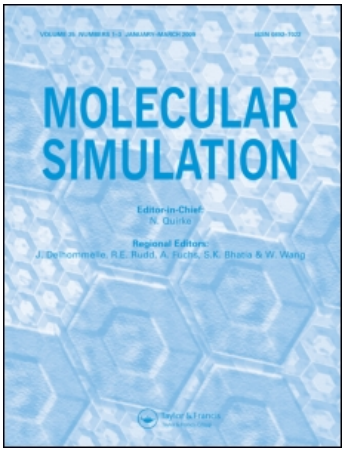

Molecular Simulation
Publication details, including instructions for authors and subscription information:
http://www.informaworld.com/smpp/title~content=t713644482

Molecular dynamics simulation of human interleukin-4: comparison with NMR data and effect of pH, counterions and force field on tertiary structure stability

M. Winger[a]; H. Yu[b]; C. Redfield[c]; W. F. van Gunsteren[a]
[a] Laboratory of Physical Chemistry, Swiss Federal Institute of Technology Zürich, ETH, Zürich, Switzerland [b] Department of Chemistry, University of Wisconsin-Madison, Madison, WI, USA [c] Department of Biochemistry, University of Oxford, Oxford, UK

To cite this Article Winger, M. , Yu, H. , Redfield, C. and van Gunsteren, W. F.(2007) 'Molecular dynamics simulation of human interleukin-4: comparison with NMR data and effect of pH, counterions and force field on tertiary structure stability', Molecular Simulation, 33: 14, 1143 — 1154
To link to this Article: DOI: 10.1080/08927020701613623
URL: http://dx.doi.org/10.1080/08927020701613623

Molecular Simulation, Vol. 33, No. 14, December 2007, 1143–1154

Taylor & Francis
Taylor & Francis Group

Molecular dynamics simulation of human interleukin-4: comparison with NMR data and effect of pH, counterions and force field on tertiary structure stability

M. WINGER†, H. YU‡, C. REDFIELD¶ and W. F. VAN GUNSTEREN†*

†Laboratory of Physical Chemistry, Swiss Federal Institute of Technology Zürich, ETH, 8093 Zürich, Switzerland
‡Department of Chemistry, University of Wisconsin-Madison, 1101 University Avenue, Madison, WI 53706, USA
¶Department of Biochemistry, University of Oxford, South Parks Road, Oxford OX1 3QU, UK

(Received April 2007; in final form August 2007)

The human protein interleukin-4 (IL-4) has been simulated at two different pH values 2 and 6, with different amounts of counterions present in the aqueous solution, and with two different force-field parameter sets using molecular dynamics simulation with the aim of validation of force field and simulation set-up by comparison to experimental nuclear magnetic resonance data, such as proton–proton nuclear Overhauser effect (NOE) distance bounds, $^3J(\mathrm{HN,HC}_\alpha)$ coupling constants and backbone N—H order parameters. Thirteen simulations varying in the length from 3 to 7 ns are compared.

At pH 6 both force-field parameter sets used do largely reproduce the NOE's and order parameters, the *GROMOS* 45A3 set slightly better than the *GROMOS* 53A6 set. ^3J values predicted from the simulation agree less well with experimental values. At pH 2 the protein unfolds, unless counterions are explicitly present in the system, but even then the agreement with experiment is worse than at pH 6. When simulating a highly charged protein, such as IL-4 at pH 2, the inclusion of counterions in the simulation seems mandatory.

Keywords: Interleukin-4; Low pH; Unfolding; Molecular dynamics simulation; Counterions

1. Introduction

During protein folding, a series of intermediate conformations are sampled prior to the appearance of the native fold. This makes an accurate description of the unfolded and the intermediate conformational states crucial to our understanding of protein folding [1–3]. Partial or complete denaturation of proteins can be achieved *in vitro* by various solution conditions, such as addition of denaturant, extremes of pH, salt concentrations or temperatures [4]. There is much interest in characterising the non-native states formed under such conditions and comparing their properties with those of globular proteins. These studies provide insights into issues such as protein 3D structure, stability and folding [5,6]. They also have significance with regard to understanding diseases associated with protein misfolding and the aggregation of non-native protein species. Such diseases include cystic fibrosis, Alzheimer's and the spongiform encephalophies [7]. Among the series of intermediate states, molten globule ensembles are of considerable interest [8,9]. A number of proteins (e.g. α-lactalbumin, carbonic anhydrase B and β-lactoglobulin) have been found to form molten globular states under mild denaturing conditions. Molten globule ensembles are characterised by having a pronounced amount of secondary structure in a compact state that lacks most of the specific tertiary interactions coming from tightly packed side-chain groups.

Interleukin-4 (IL-4) is a pleiotropic type 1 cytokine, which plays a central role in the control and regulation of the immune and inflammatory systems [10]. The most notable functions of IL-4 include the development of T-helper cells to a type 2 cytokine-producing phenotype. IL-4 evokes a cellular response by promoting the formation of a heterodimeric receptor complex in the plasma membrane [11–13]. The 3D structure of IL-4 under native conditions has been established in solution [14,15] and in crystals [16–18]. IL-4 is one of the four helix bundle cytokines [19] that are characterised by antiparallel juxtaposed helices A, B, C, D and two long end-to-end

*Corresponding author. Tel.: + 41-44-632-5502. Fax: + 41-44-632-1039. Email: wfvgn@igc.phys.chem.ethz.ch; igc-sec@igc.phys.chem.ethz.ch

Molecular Simulation
ISSN 0892-7022 print/ISSN 1029-0435 online © 2007 Taylor & Francis
http://www.tandf.co.uk/journals
DOI: 10.1080/08927020701613623

loops, loops AB and CD, which are connected by a short β-sheet packed against helices B and D. Human IL-4 has six cysteine residues which form three disulfide bonds (C3-C127, C24-C65, C46-C99). The overall structure is highly compact and globular with a predominantly hydrophobic core. Smith *et al.* [20] have thoroughly compared the four independently determined structures of human recombinant IL-4 and they found the core of the four helix bundle to be very similar in all the structures, except for differences in loop regions that are known to be mobile in solution [21]. At low pH (e.g. at pH ≈ 2.4), it was found experimentally that IL-4 undergoes a partial unfolding transition [22]. Comparison of the nuclear magnetic resonance (NMR) spectra of IL-4 at pH 5.6 and pH 2.4 shows that the pattern of chemical shifts and nuclear Overhauser effect (NOE's) is little changed for the majority of the residues. Therefore, at low pH IL-4 appears to retain a highly ordered hydrophobic core in which most, but not all, secondary structure is preserved. However, extensive disorder exists in the loop regions of the polypeptide chain that link these secondary structural elements; at pH 2.4 these mobile loop regions represent more than one third of the protein residues. This low pH form has been described as a highly-ordered molten globule [22].

Despite extensive experimental studies, detailed insight into the low pH molten globule state of IL-4 is still lacking. For example, the diversity of conformations in the disordered loops and the rearrangement of secondary structure between pH 5.6 and 2.4 have not been well characterised.

Previously, MD simulation has been used to study the properties of the molten globule state of various proteins, including hen egg white lysozyme [23], bovine pancreatic trypsin inhibitor [24], α-lactalbumin [25,26]. MD simulation was used in the present study to investigate in atomic detail the structural and dynamic properties of IL-4 at low pH. Various properties obtained from simulation trajectories at low pH will be compared with those at pH 6 and with the corresponding experimental NMR data.

In practice, counterions are usually not included in protein simulations, mainly because they diffuse slowly in the simulation and their initial positioning might have significant effects on the simulation trajectory [27]. The underlying thought is that features, e.g. the counterion positional distribution, that will not converge within accessible simulation time are better omitted or, in other words, included in a mean-field manner in the simulation. Secondly, in explicit water simulations the water molecules of the first few coordination layers very effectively shield the ions, as can be observed from radial distribution functions. Thus for proteins with a relatively low overall charge with respect to their size or number of residues, omission of counterions is a reasonable first-order approximation of co-solvent effects. In the literature, contradictory results are reported regarding the effects of counterions on the stability of a protein fold in simulations [28–31]. Ibragimova and Wade [28] found that explicit modelling of 0.2 M ionic strength is necessary to maintain the stable structure for the YAP-WW domain. Martí-Renom *et al.* [29] found that inclusion of counterions contributes to preserve the native structure in the simulation of the activation domain of procarboxypeptidase B. However, Drabik *et al.* [31] found that simulations of solvated proteins are only moderately sensitive to the presence of counterions. This sensitivity was reported to be highly dependent on the starting structures and the different equilibration procedures used.

For IL-4, the different pH values, mimicked by setting proper protonated states of the ionizable residues, lead to highly charged proteins, +11 *e* at pH 6 and +27 *e* at pH 2, while the 129-residue protein is relatively small. Therefore, apart from pH effects, we also investigate the effect of the counterions on the stability of this protein in the simulations.

The quality of a biomolecular simulation will depend on the force field used. Current widely used biomolecular force fields are AMBER [32–34], CHARMM [35–37], OPLS-AA [38,39] and *GROMOS* [40–42]. Not long ago, it was shown that all of these force fields severely underestimate the free energy of hydration for series of small molecules that represent the amino acid side chains [43–45]. For this reason a parametrisation of the *GROMOS* force field was carried out which led to the 53A6 parameter set [46]. Here we use both sets, the 45A3 [42] and the 53A6 one, in order to see how the new set derived from free energies of hydration and solvation will perform for IL-4.

2. Methods

2.1 Molecular dynamics simulations

MD simulations were performed with the *GROMOS* software package [41,47] using the force-field parameter sets 45A3 [42] and 53A6 [46]. The 13 MD simulations are summarised in table 1. Initial coordinates were taken from the X-ray structure of IL-4 (Protein data bank entry: 1RCB) [16]. The different pH values were mimicked by different protonation states of protonisable residues [25]: Asp, Glu and C-terminus are not protonated at pH 6 while protonated at pH 2; His is protonated at both pH's except for His76 which at pH 6 is only protonated at N_ϵ. The simple-point-charge (SPC) water model [48] was used to describe the solvent molecules. In the simulations, water molecules were added around the protein within a truncated octahedron with a minimum distance of 1.4 nm between the protein atoms and the square walls of the periodic box. In some of the simulations, ions (Cl^- and Na^+) were included. Cl^- ions were introduced by replacing the water molecules with the highest electrostatic potential and Na^+ by replacing the water molecules with the lowest electrostatic potential. The electrostatic potential at the oxygen atoms of the water molecules was calculated by taking into account all the atoms within the spherical shell of water with a cutoff

Table 1. Overview of the simulations performed.

Simulation label	*Force-field parameter set*	*pH*	*Number of counterions*	*Protein total charge [e]*	*Simulation length [ns]*
pH6_45A3	45A3	6	–	+ 11	4
pH6_53A6	53A6	6	–	+ 11	4
pH6_45A3_REF	45A3	6	–	+ 11	4
pH6_45A3_6Cl	45A3	6	6 Cl^-	+ 5	7
pH6_45A3_11Cl	45A3	6	11 Cl^-	0	4
pH6_45A3_20Cl_9Na	45A3	6	20 Cl^- 9 Na^+	0	7
pH6_45A3_30Cl_19Na	45A3	6	30 Cl^- 19 Na^+	0	4
pH2_45A3	45A3	2	–	+ 27	4
pH2_53A6	53A6	2	–	+ 27	4
pH2_45A3_REF	45A3	2	–	+ 27	4
pH2_45A3_16Cl	45A3	2	16 Cl^-	+ 11	3
pH2_45A3_21Cl	45A3	2	21 Cl^-	+ 6	3
pH2_45A3_27Cl	45A3	2	27 Cl^-	0	4

Two *GROMOS* [41,47] force-field parameter sets, 45A3 [42] and 53A6 [46] were used in the simulations. The pH-values indicate different charge states for the ionizable (side-chain) moieties. In simulations pH6_45A3_REF and pH2_45A3_REF initially 100 ps of MD simulation was performed with proton–proton NOE upper-bound distance restraining, as in NMR structure refinement.

1.4 nm. The minimal distance between the protein atoms and the ions was set to be 0.35 nm. All the bonds were constrained with a geometric tolerance of 10^{-4} using the SHAKE algorithm [49]. A steepest-descent energy minimisation of the systems was performed to relax the solute–solvent contacts, while positionally restraining the solute atoms using a harmonic interaction with a force constant of $2.5 \times 10^4\,\mathrm{kJ\,mol^{-1}\,nm^{-2}}$. Next, steepest-descent energy minimisation of the system without any restraints was performed to eliminate any residual strain. The energy minimisations were terminated when the energy change per step became smaller than $0.1\,\mathrm{kJ\,mol^{-1}}$. For the non-bonded interactions, a triple-range method with cutoff radii of 0.8/1.4 nm was used. Short-range van der Waals and electrostatic interactions were evaluated every time step based on a charge-group pairlist. Medium-range van der Waals and electrostatic interactions, between pairs at a distance longer than 0.8 nm and shorter than 1.4 nm, were evaluated every fifth time step, at which time point the pair list was updated. Outside the longer cutoff radius a reaction-field approximation [50] was used with a relative dielectric permittivity of 66 [51]. The initial velocities of the atoms were assigned from a Maxwell distribution at 50 K. Five picoseconds periods of MD simulation with harmonic position restraining of the solute atoms with force constants of $2.5 \times 10^4\,\mathrm{kJ\,mol^{-1}\,nm^{-2}}$, $2.0 \times 10^{-4}\,\mathrm{kJ\,mol^{-1}\,nm^{-2}}$, $1.5 \times 10^{-4}\,\mathrm{kJ\,mol^{-1}\,nm^{-2}}$, $1.0 \times 10^{-4}\,\mathrm{kJ\,mol^{-1}\,nm^{-2}}$, $0.5 \times 10^{-4}\,\mathrm{kJ\,mol^{-1}\,nm^{-2}}$ were performed to equilibrate further the systems at 50, 150, 250, 308 and 308 K, respectively. During the equilibration, solvent and solute were independently, weakly coupled to a temperature bath of the given temperature with a relaxation time of 0.1 ps [52]. In the further simulations, the center of mass motion of the whole system was removed every 1000 time steps. The systems were also weakly coupled to a pressure bath of one atom with a relaxation time of 0.5 ps and an isothermal compressibility of $0.4575 \times 10^{-3}\,(\mathrm{kJ\,mol^{-1}\,nm^{-3}})^{-1}$. The trajectory coordinates and energies were saved every 0.5 ps for analysis.

For a highly charged protein, the use of an appropriate method to treat long-range electrostatic interactions, such as lattice-sum or reaction-field methods, is mandatory. Both, lattice-sum methods (Ewald, P3M, etc.) and reaction-field methods (dipolar, time-dependent, etc.) to treat long-range electrostatic interactions cause artefacts in molecular simulations, the former because of their artificial enhancement of periodic order and the latter because of their mean-field character. Since, we judge the former artefacts to be more severe than the latter [53–59] we applied the reaction-field methodology in the present study.

2.2 Structural refinement with nuclear Overhauser effect restraints

In two simulations (carrying "REF" in their name in table 1) a short period of 100 ps of structural refinement with explicit solvent MD simulation was performed using instantaneous NOE upper-bound distance restraining [60] in order to be sure that these restraints are fulfilled at the start of these simulations. In this case, in addition to the physical potential energy a restraining potential-energy term

$$V_{\mathrm{dr}}(r_{ij}) = \begin{cases} \frac{1}{2}K_{\mathrm{dr}}(r_{ij} - r_{ij}^0)^2 & \text{if} \quad r_{ij} > r_{ij}^0 \\ 0 & \text{if} \quad r_{ij} \le r_{ij}^0 \end{cases} \qquad (1)$$

is used, where K_{dr} is the force constant for the distance restraining, r_{ij} is the instaneous distance between atoms i and j, and r_{ij}^0 is the reference distance, i.e. the NOE upper-bound distance. The force constant K_{dr} was chosen to be $2000\,\mathrm{kJ\,mol^{-1}\,nm^{-2}}$. In the *GROMOS* force-field parameter sets 45A3 [42] and 53A6 [46], aliphatic hydrogen atoms are not explicitly treated but are part of united atoms. We thus calculate interproton distances involving the aliphatic hydrogen atoms by calculating virtual (for CH_1 and prochiral CH_2) [61] and pseudo (for CH_3) [62] atomic positions for these hydrogen atoms [41]. When comparing the experimentally derived distances with the calculated proton–proton distances, pseudo-atom corrections involving equivalent or nonstereospecifically

assigned protons should be included in the NOE-derived upper-bound distances. The same corrections as used in the structure determination of IL-4 [14,22,62] are used in our study.

2.3 Analysis

Analyses of the trajectory configurations were done with the analysis software *GROMOS++* [63] and esra [64].

Atom-positional root-mean-square differences between structures were calculated by performing a rotational and translational atom-positional least-squares fit of one structure on the second (reference) structure using a given set of atoms. Atom-positional root-mean-square fluctuations (RMSFs) over a period of simulation were calculated by performing a rotational and translational atom-positional least-squares fit of the trajectories on the reference structure (usually the first structure of the period) using a given set of atoms. The secondary structure assignment was done using the program DSSP, based on the Kabsch–Sander rules [65].

Comparisons to NMR experimental data were made through an analysis of proton–proton distances as compared to NOE upper bounds, of ^3J(HN, HC$_\alpha$) coupling constants and of ^{1}H—^{15}N order parameters. For pH 5.6 [14], 1656 NOE upper bounds were available and for pH 2.4, 1450 NOE upper bounds [22]. Proton–proton distances were averaged using $1/r^3$ averaging, using $\bar{r} = (\langle r^{-3}\rangle)^{-1/3}$, corresponding to a slowly tumbling molecule [66]. ^3J-coupling constants were calculated from the simulations using the Karplus relation [67],

$$^3J(H,H) = a\cos^2\theta + b\cos\theta + c \qquad (2)$$

The parameters a, b, c used were: $a = 6.51$ Hz, $b = -1.76$ Hz and $c = 1.60$ Hz [68] for calculating ^3J(HN, HC$_\alpha$) values.

According to their definition, generalised order parameters S^2 may be directly calculated from a simulation using the long-time tail of the second-order Legendre function of the reorientation correlation function of the N—H vector ($\vec{v}$):

$$S^2 = \lim_{t\to\infty} C_2(t) \qquad (3)$$

where

$$C_2(t) = \langle P_2(\vec{v}(\tau)\cdot\vec{v}(\tau+t))\rangle_\tau \qquad (4)$$

Here P_2 is the second-order Legendre polynomial, $P_2(x) = 1/2(3x^2 - 1)$. The angular brackets (<>) represent the average over the ensemble (trajectory). The unit vectors $\vec{v}(\tau)$ and $\vec{v}(\tau + t)$ describe the orientation of the N—H vector at times τ and $\tau + t$ in relation to a fixed reference frame. To construct this frame, the translational and overall rotational motions were removed by a root-mean-square fitting of all backbone atoms onto the starting conformation. In practice, expressions (3) and (4) are not very suitable to obtain accurate results, since the long-time tail of a correlation function is generally plagued by poor statistics. Therefore, the alternative formula [69,70]

$$S^2 = \frac{1}{2}\left[3\sum_{\alpha=1}^{3}\sum_{\beta=1}^{3} < v_\alpha(t)v_\beta(t) >_t^2 - 1\right] \qquad (5)$$

is used, which involves trajectory averages of the elements $v_\alpha v_\beta$ of the Cartesian tensor built as a direct product of the Cartesian components of the unit vector $\vec{v}(t)$, and yields, therefore, more precise results. The average of S^2 is either taken over all configurations at 0.5 ps intervals of the whole simulation [71–73].

Diffusion constants have been calculated via the Einstein-formula

$$D = \lim_{t\to\infty} \frac{\langle (r(t+\tau) - r(\tau))^2\rangle_\tau}{6t} \qquad (6)$$

3. Results and discussion

3.1 IL-4 at pH 6

The atom-positional root-mean-square deviations (RMSDs) from the starting coordinates for the atoms (N, C$_\alpha$, C) in the simulations pH6_45A3, pH6_53A6 and pH6_45A3_REF are shown in figure 1. The RMSD values for all three simulations reach a plateau value of 0.2 nm after 0.5–1 ns and fluctuate around that value afterwards. The atom-positional RMSFs for the C$_\alpha$ atoms were calculated for the whole 4 ns of the trajectories (figure 2). These three simulations show larger fluctuations in loop regions (i.e. loops AB and CD) while smaller fluctuations in the helical parts. Generally, the simulations using force-field parameter sets 45A3 [42] and 53A6 [46] show comparable behaviour although the 53A6 parameter set seems to favour 3_{10}-helical structure slightly more and α-helical structure slightly less than the 45A3 set. The secondary structure assignment shows that the helical

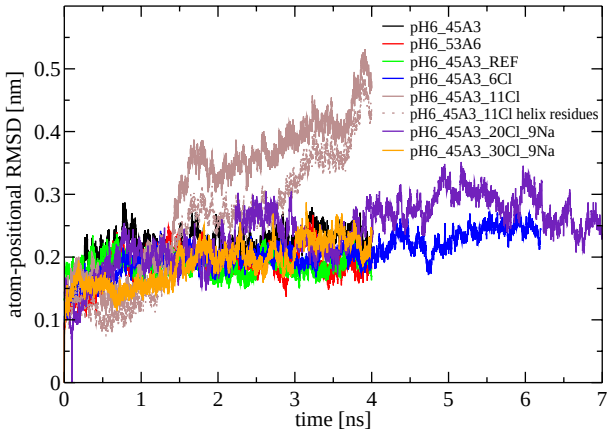

Figure 1. Atom-positional RMSDs of the backbone atoms (N, C$_\alpha$, C) of IL-4 with respect to the starting (X-ray) structure in the simulations pH6_45A3 (black), pH6_53A6 (red) and pH6_45A3_REF (green), pH6_45A3_6Cl (blue), pH6_45A3_11Cl (brown), pH6_45A3_11Cl helix residues (brown dotted), pH6_45A3_20Cl_9Na (purple) and pH6_45A3_30Cl_19Na (orange) (colour in online version).

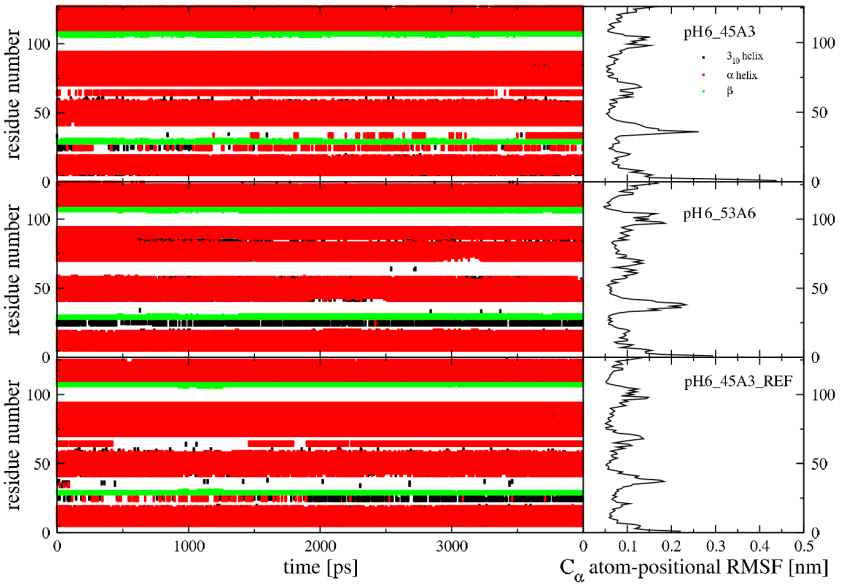

Figure 2. Secondary structure elements (left panels) and atom-positional RMSFs of the C_α atoms (right panels) of IL-4 over the simulations pH6_45A3 (upper panels), pH6_53A6 (middle panels) and pH6_45A3_REF (lower panels). α-helix (red), 3_{10}-helix (black) and β-strand (green) (colour in online version).

structural elements are very stable in these three simulations. Some rearrangement in the loops was observed. In figure 3 the final conformations from these three simulations are shown. The overall secondary structure is well preserved in the three simulations with the different force-field parameter sets.

A summary of the NOE analysis can be found in table 2, while NOE distance distributions are displayed in figure S1 of the supplementary material. A total of 1656 NOE upper bounds were used in the analysis for pH 6 [14]. The three simulations without counterions satisfy more than 98% of the experimental upper bounds within 0.1 nm. Applying NOE restraints for the first 0.1 ns (pH6_45A3_REF) only slightly reduces the number of violations and the average violation. The simulation pH6_45A3 shows somewhat lower violations compared to the simulation pH6_53A6. One of the two observed larger NOE violations (larger than 0.3 nm averaged over 1.0–4.0 ns) using the 53A6 parameter set occurs in loop AB (35AlaH$_\alpha$–38AsnHN) and the other is related to 63Thr in the loop between helix B and C. Figure 3 shows the experimentally derived crystal structure (PDB entry: 1RCB [16]) and solution structure (PDB entry: 1ITM [14]). There exists a large difference for the BC and CD loops between the crystal structure and the solution structure. The simulations, which started from the crystal structure, may not have allowed these loops to explore all their conformational possibilities such that the observed NOE bounds are satisfied.

Three-bond ^3J(HN, HC$_\alpha$) coupling constants have been calculated from the simulation ensembles and were compared against experimental values (table 3 and figure S2 of the supplementary material). ^3J coupling constants were reported for 114 residues of which 46 were upper bounds [14]. The two parameter sets 45A3 and 53A6 give comparable results. Applying NOE upper-bound distance restraining for the first 0.1 ns does not improve the agreement. Generally ^3J(HN, HC$_\alpha$) coupling constants are less well reproduced than other NMR properties [74], which might have different reasons: (i) the time scale needed to achieve converged sampling for ^3J-values from MD simulations may be much beyond a few nanoseconds, (ii) the intrinsic problem of the accuracy of the empirically calibrated Karplus relation and (iii) the difficulty of obtaining reliable ϕ-torsional angle potential-energy terms for amino-acid residues.

Backbone N—H order parameters calculated from the MD simulations averaged over 0.0–4.0 ns are compared with experimental data [21] in figure 4. All three simulations without counterions show similar amplitudes and profiles with respect to N—H mobility and reproduce the experimental variations. On average, the experimental order parameters are slightly larger than those obtained from the simulations.

In short we can conclude that MD simulations at pH 6 with two force-field parameter sets both reproduced various experimentally derived properties well, except for the ^3J(HN, HC$_\alpha$) values for which about one third showed violations of more than 1 Hz.

3.2 IL-4 at pH 2

The atom-positional RMSDs from the initial X-ray structure for the backbone atoms (N, C$_\alpha$, C) in the simulations pH2_45A3, pH2_53A6 and pH2_45A3_REF are shown in figure 5. The RMSD values increase to around 1.5 nm, a value much larger than those in the simulations at pH 6. This means that the starting structure is far from the equilibrium ensemble sampled by MD at low pH. Since the starting structure was the X-ray crystal structure which was determined at pH 6.0, we applied

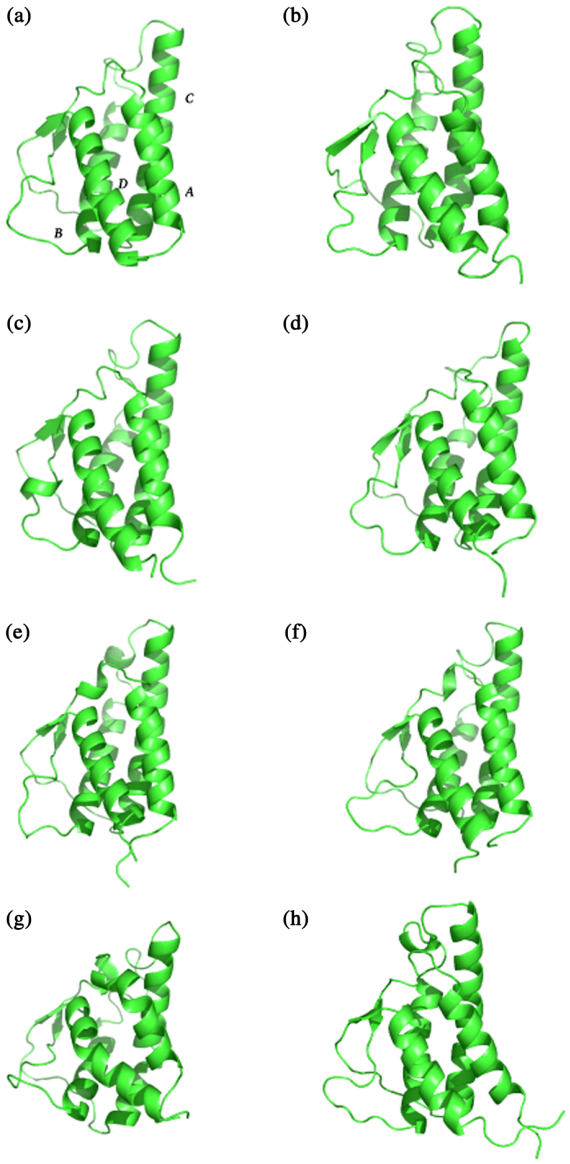

Figure 3. The X-ray structure (a) and NMR solution structure (b) of IL-4 are shown with the four helices A–D indicated. Structures of IL-4 at pH 6 at the end of simulations pH6_45A3 (c), pH6_53A6 (d), pH6_45A3_REF (e), pH6_45A3_6Cl (f), pH6_45A3_11Cl (g) and pH6_45A3_20Cl_9Na (h).

distance restraining with NOE bounds derived from the NOE intensities determined at pH 2 [22] for the first 0.1 ns (simulation pH2_45A3_REF). This did not keep the structure stable, similar unfolding behaviour was observed. The atom-positional RMSF for the C_α atoms were calculated for the entire simulation periods (figure 6). In all three simulations without counterions much larger fluctuations were observed compared to those of the simulations at pH 6. A large amount of the secondary structure was lost in all three simulations, which is in contrast to what has been found experimentally.

Not surprisingly, large NOE violations were observed in all three simulations without counterions (table 2) due to the unfolding of the compact structure. Both the ^3J-coupling constants and the N—H order parameters were not well reproduced in the simulations.

3.3 *Effects of counterions at pH 6*

In the present study, the protonation states of the protonisable residues are assigned according to the pK_a of the side chain without taking into account the protein environment and the possible variation of the local pH value. With this simple method, the total charges of IL-4 at pH 6 and 2 are $+11$ e and $+27$ e, respectively. The high net charges, especially at pH 2 may have a large effect on the stability of the protein. Addition of neutralizing counterions or additionally increasing the ionic strength of the solution may reduce a dominating influence of the protein charge on its behaviour.

In figure 1 backbone (N, C_α, C) RMSDs with respect to the starting structure are shown for the simulations pH6_45A3_6Cl, pH6_45A3_11Cl, pH6_45A3_ 20Cl_9Na and pH6_45A3_30Cl_19Na. Significant deviation from the starting structure is only observed for the simulation pH6_45A3_11Cl, the others show values around 0.25 nm, as in the simulations without counterions. The deviation for pH6_45A3_11Cl arises from structural changes between the helices (figure 1).

As seen in figure 7 the secondary structure features of the simulation pH6_45A3_11Cl remain intact, the C_α-atom positional RMSF in the helix regions still being

Table 2. Number of NOE upper distance bound violations and average violations in the simulations for given time periods. At pH 6 a total number of 1656 NOE's and at pH 2 a total of 1450 NOE's were considered.

		Number of NOE upper bound violations			
Simulation label	*Averaging time period (ns)*	*≥ 0.1 (nm)*	*≥ 0.2 (nm)*	*≥ 0.3 (nm)*	*Average violations (nm)*
pH6_45A3	1–4	19	1	1	0.004
pH6_53A6	1–4	30	3	2	0.006
pH6_45A3_REF	1–4	16	3	0	0.003
pH6_45A3_6Cl	1–7	23	3	1	0.004
pH6_45A3_11Cl	1–4	23	7	2	0.004
pH6_45A3_20Cl_9Na	1–7	36	12	9	0.007
pH6_45A3_30Cl_19Na	1–4	20	3	1	0.004
pH2_45A3	1–4	183	141	115	0.114
pH2_53A6	1–4	464	357	297	0.227
pH2_45A3_REF	1–4	131	45	7	0.019
pH2_45A3_16Cl	1–3	82	43	22	0.047
pH2_45A3_21Cl	1–3	84	58	55	0.038
pH2_45A3_27Cl	1–4	45	28	17	0.011

Table 3. Number of $^3J_{HN\alpha}$-coupling constants for which the absolute difference between the experimentally determined $^3J_{HN\alpha}$-coupling constants and the calculated $^3J_{HN\alpha}$-coupling constants averaged over the MD trajectories is larger than a given value. Only 68 ^3J-coupling constants with exact experimental values have been considered.

		Number of J-values with $\lvert J_{exp}\text{-}J_{sim}\rvert$			
Simulation label	*Averaging period [ns]*	≥ 1 *Hz*	≥ 2 *Hz*	≥ 3 *Hz*	≥ 4 *Hz*
pH6_45A3	1–4	27	12	3	0
pH6_53A6	1–4	26	11	6	1
pH6_45A3_REF	1–4	22	7	3	1
pH6_45A3_6Cl	1–4	25	12	6	1
pH6_45A3_11Cl	1–4	21	7	1	1
pH6_45A3_20Cl_9Na	1–7	24	10	2	1
pH6_45A3_30Cl_19Na	1–4	22	6	2	1

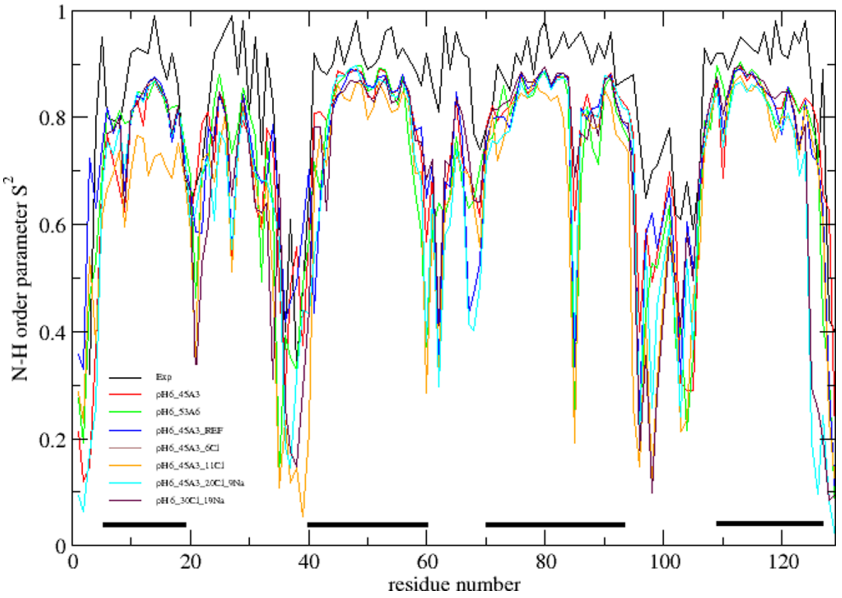

Figure 4. Backbone N—H order parameter S^2 as a function of the residue sequence number. The averages were calculated over the entire simulation time. Black line: experimental values [21]; Red line: simulation pH6_45A3; Green line: simulation pH6_53A6; Blue line: simulation pH6_45A3_REF. Brown line: simulation pH6_45A3_6Cl. Orange line: simulation pH6_45A3_11Cl. Turquoise line: simulation pH6_45A3_20Cl_9Na. Purple line: simulation pH6_45A3_30Cl_19Na. The four helices are indicated by horizontal black bars (colour in online version).

higher than in the other three simulations at pH 6 with counterions (figure 7). Figure 3 shows the reference structure and the structure at the end of simulation pH6_45A3_11Cl. The elevated RMSD and RMSF values seem to arise from a kink in helix C.

In table 2 the NOE upper distance bound violations for the simulations with ions are shown. The average violations are similar to those in the simulations without ions at pH 6, even though there are more distance violations than in the simulation pH6_45A3.

In table 3 the average ^3J-coupling constant violations are shown. The simulations with counterions show a similar number of violations as the simulations without ions, except at high ionic strength, simulation pH6_45A3_30Cl_19Na. The backbone N—H order parameters (figure 4) show similar profiles with respect to N—H mobility in all simulations.

Diffusion constants for chloride and sodium ions have been calculated (table S1, supplementary material). For

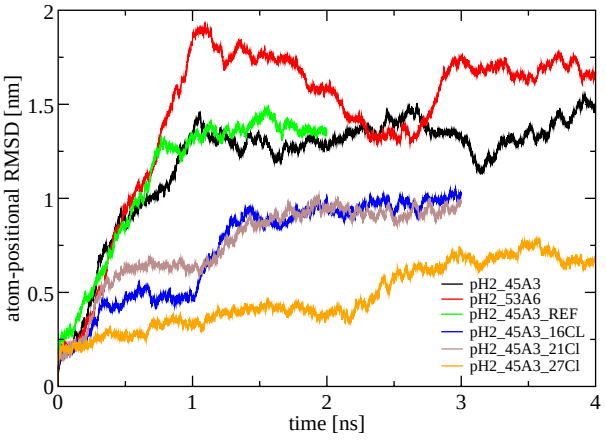

Figure 5. Atom-positional RMSDs of the backbone atoms (N, C_α, C) of IL-4 with respect to initial (X-ray) structure in the simulations pH2_45A3 (black), pH2_53A6 (red) and pH2_45A3_REF (green), pH2_45A3_16Cl (blue), pH2_45A3_21Cl (brown) and pH2_45A3_27Cl (orange) (colour in online version).

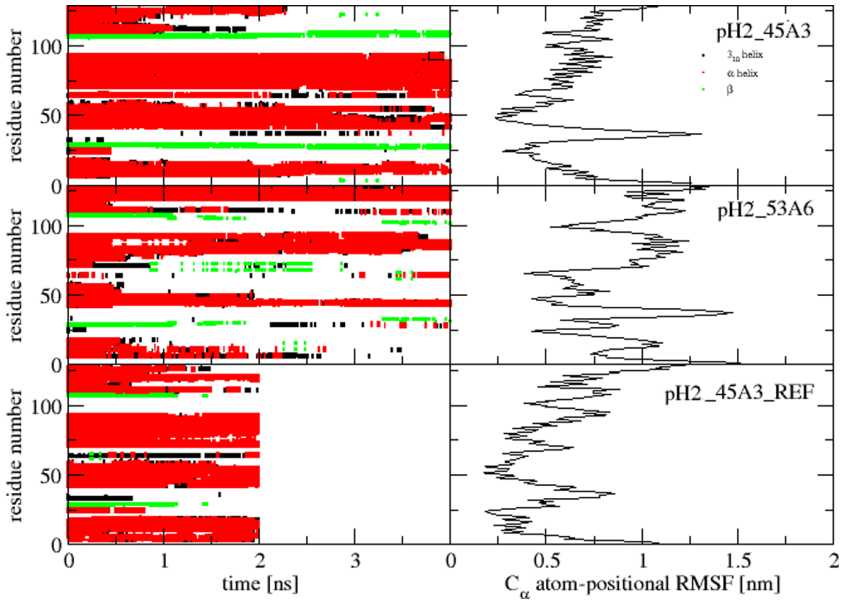

Figure 6. Secondary structure elements (left panels) and atom-positional RMSFs of the C_α atoms (right panels) of IL-4 in the simulations pH2_45A3 (upper panels), pH2_53A6 (middle panels) and pH2_45A3_REF (lower panels). α-helix (red), 3_{10}-helix (black) and β-strand (green).

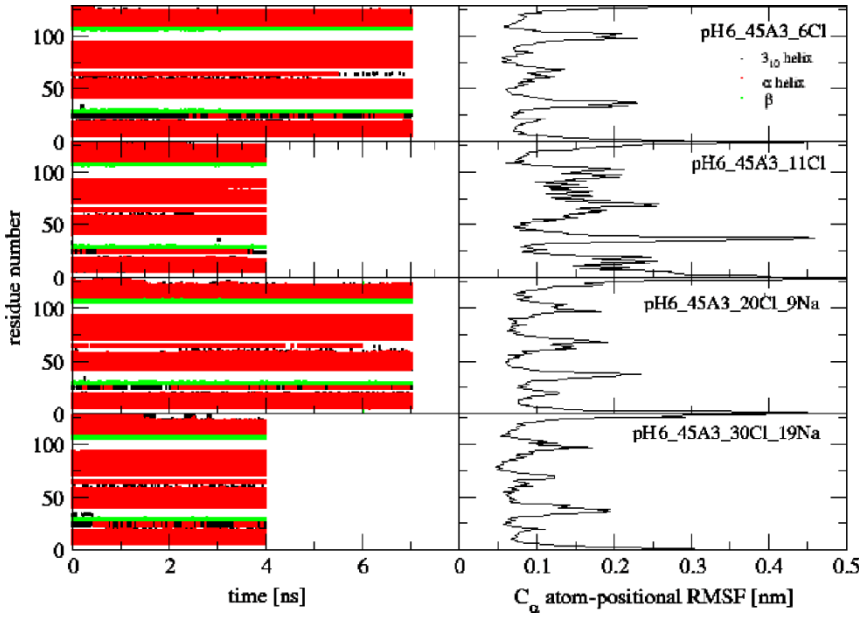

Figure 7. Secondary structure elements (left panels) and atom-positional RMSFs of the C_α atoms (right panels) of IL-4 in the simulations pH6_45A3_6Cl, pH6_45A3_11Cl, pH6_45A3_20Cl_9Na and pH6_45A3_30Cl_19Na. α-helix (red), 3_{10}-helix (black) and β-strand (green) (colour in online version).

chloride the values are of the same order of magnitude as the experimentally determined diffusion constants of the ions at 298 K in water ($D^-_{Cl} = 2.03 \times 10^{-5}\,cm^2/s$ [75], $D^+_{Na} = 1.33 \times 10^{-5}\,cm^2/s$ [76]). The sodium ions diffuse too fast ($2.4–4.1 \times 10^{-5}\,cm^2/s$) in the simulations.

3.4 Effects of counterions at pH 2

The N, C_α, C atom-positional RMSDs for the simulations pH2_45A3_16Cl, pH2_45A3_21Cl and pH2_45A3_27Cl with respect to the starting structure are shown in figure 5. The RMSD values are significantly smaller than the values obtained from simulation without ions at the same pH. The simulations pH2_45A3_16Cl and pH2_45A3_21Cl converge to an RMSD-value of 1 nm, the simulation pH2_45A3_27Cl to a value somewhat lower (0.7 nm). The protein's secondary structure features (figure 8) stay intact during the simulation period except for partial unfolding of the A helix in simulations pH2_45A3_16Cl and pH2_45A3_21Cl and of the D helix in simulations pH2_45A3_16Cl and pH2_45A3_27Cl. As expected the atom-positional RMS fluctuations are

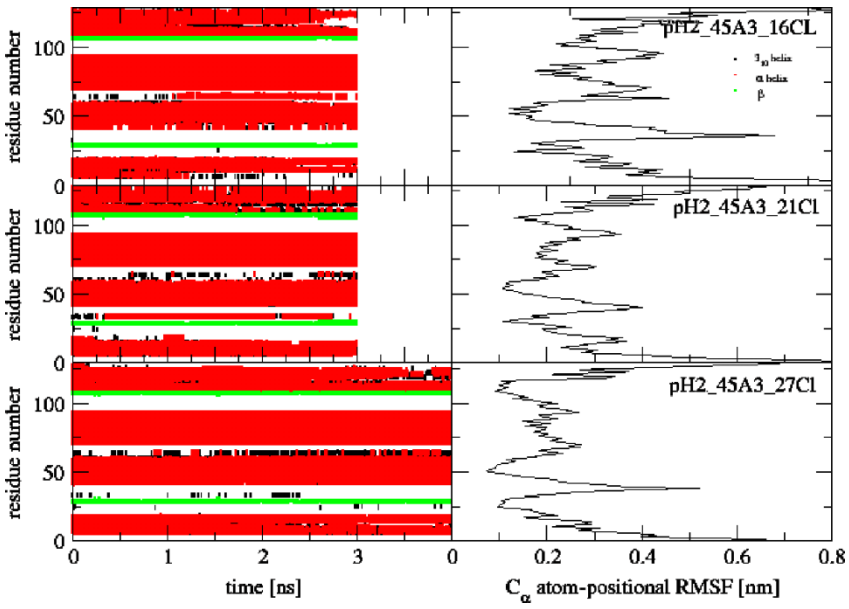

Figure 8. Secondary structure elements (left panels) and atom-positional RMSFs of the C_α atoms (right panels) of IL-4 in the simulations pH2_45A3_6Cl (upper panels), pH2_45A3_21Cl (middle panels) and pH2_45A3_27Cl (lower panels). α-helix (red), 3_{10}-helix (black) and β-strand (green) (colour in online version).

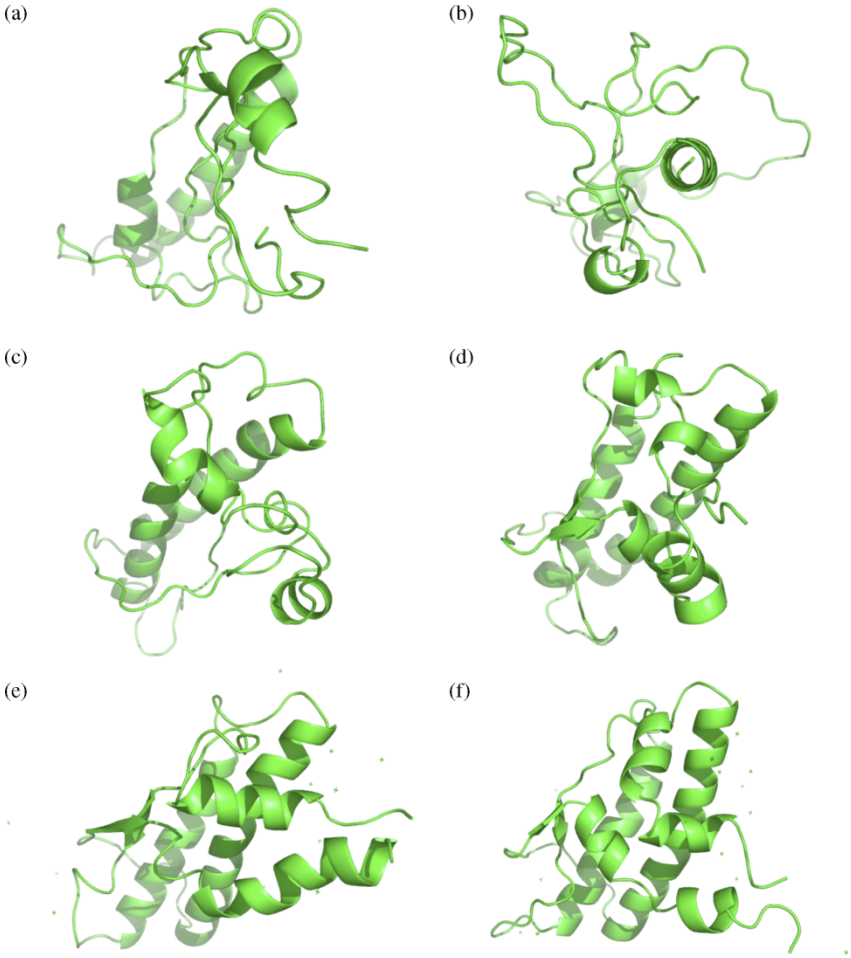

Figure 9. Structures of IL-4 at pH 2 at the end of simulations pH2_45A3 (a), pH2_53A6 (b), pH2_45A3_REF (c), pH2_45A3_16Cl (d), pH2_45A3_21Cl (e) and pH2_45A3_27Cl (f).

smaller than in the simulations without counterions (figure 9).

The NOE violations are summarised in table 2. A total number of 1450 experimental upper bounds has been used. Compared to the simulations without counterions there are significantly fewer violations and the average violations are smaller for the ionic simulations. Yet, at pH 2 the average violations and the number of violations are much larger than at pH 6. The N—H order parameters also show sizeable deviations from experiment (results not shown).

4. Discussion

This work presents the results of molecular dynamics simulations of IL-4 using the *GROMOS* force-field parameter sets 45A3 and 53A6. Comparison of simulated and measured NMR data (NOE's, ^3J(HN, HC_α)-values, N—H S^2-values) has been done to evaluate the performance of the more recent force-field parameter set 53A6.

Generally, at pH 6 the parameter sets 45A3 and 53A6 yield similar results, although the former seems to reproduce experimental values slightly better. Use of NOE restraints during the first 0.1 ns of simulation does not significantly improve agreement with experiment.

Counterions were added to the simulated system in order to monitor the protein stability as a function of ionic strength at two different pH values. At pH 6 the protein stability seems to be neither increased nor decreased significantly by the introduction of counterions. Atom-positional deviations from the starting X-ray structure converge to similar values, except in the case where helix C becomes kinked after the introduction of 11 chloride ions (pH6_45A3_11Cl). Atom-postional fluctuations are also similar with and without counterions, secondary structure elements are stable in both cases. The behaviour of simulation pH6_45A3_11Cl gives an indication that the initial placement of counterions followed by an extensive MD equilibration phase with the solute restrained is crucial. Otherwise, the high charge of an ion being initially positioned close to a charged protein atom may seriously alter the protein structure already at the beginning of the simulation.

At low pH, however, the stability of IL-4 is dramatically increased by the introduction of counterions as is reflected in the atom-positional deviations from the starting structure and the secondary structure evolution. The presence of counteracting charges in the solution around the protein's net charge seems to infer stability by reducing the effective repulsive interactions between charges in the protein. In the present study no clear correlation between protein stability and ionic strength could be observed. At pH 6 the agreement between simulation and experiment degrades somewhat upon increasing the ionic strength of the solution, whereas at pH 2 the opposite effect is observed.

Finally we conclude that ions have a positive influence on a highly charged protein's stability in simulation if the initial placement of the ions is chosen well and their distribution is equilibrated with MD with the solute restrained for a sufficiently long time.

Acknowledgements

We thank Theresa Soares for fruitful discussions. Financial support was obtained from the National Center of Competence in Research (NCCR) Structural Biology of the Swiss National Science Foundation, which is gratefully acknowledged.

References

[1] W.F. van Gunsteren, R. Bürgi, C. Peter, X. Daura. The key to solving the protein-folding problem lies in an accurate description of the denatured state. *Angew. Chem. Int. Ed. Eng.*, **40**, 351 (2001).
[2] A.R. Dinner, M. Karplus. Comment on the communication. The key to solving the protein-folding problem lies in an accurate description of the denatured state by van Gunsteren *et al*. *Angew. Chem. Int. Ed. Eng.*, **40**, 4615 (2001).
[3] W.F. van Gunsteren, R. Bürgi, C. Peter, X. Daura. Reply to the comment on the communication by van Gunsteren *et al*. *Angew. Chem. Int. Ed. Eng.*, **40**, 351 (2001) *Angew. Chem. Int. Ed.*, **40**, 4616–4618, 2001.
[4] C. Tanford. Protein denaturation. *Adv. Protein Chem.*, **23**, 121 (1968).
[5] K.A. Dill, D. Shortle. Denatured states of proteins. *Annu. Rev. Biochem.*, **60**, 795 (1991).
[6] C.M. Dobson. Unfolded proteins, compact states and molten globules. *Curr. Opin. Struct. Biol.*, **2**, 6 (1992).
[7] C.M. Dobson. Principles of protein folding, misfolding and aggregation. *Semin. Cell Dev. Biol.*, **15**, 3 (2004).
[8] C.M. Dobson. Protein-folding—solid evidence for molten globules. *Curr. Biol.*, **4**, 636 (1994).
[9] M. Arai, K. Kuwajima. Role of the molten globule state in protein folding. *Adv. Protein Chem.*, **53**, 209 (2000).
[10] W.E. Paul. Interleukin-4: a prototypic immunoregulatory lymphokine. *Blood*, **77**, 1859 (1991).
[11] K. Nelms, A.D. Keegan, J. Zamorano, J.J. Ryan, W.E. Paul. The IL-4 receptor: signaling mechanisms and biologic functions. *Annu. Rev. Immunol.*, **17**, 701 (1999).
[12] R.A. Seder, W.E. Paul. Acquisition of lymphokine-producing phenotype by CD4 + T-cells. *Annu. Rev. Immunol.*, **12**, 635 (1994).
[13] P. Reinemer, W. Sebald, A. Duschl. The interleukin-4-receptor: from recognition mechanism to pharmacological target structure. *Angew. Chem. Int. Ed. Eng.*, **39**, 2834 (2000).
[14] L.J. Smith, C. Redfield, J. Boyd, G.M.P. Lawrence, R.A.G. Smith, C.M. Dobson. Human interleukin-4: the solution structure of a 4-helix bundle protein. *J. Mol. Biol.*, **224**, 899 (1992).
[15] R. Powers, D.S. Garrett, C.J. Marchand, E.A. Frieden, A.M. Gronenborn, G.M. Clore. 3-dimensional solution structure of human interleukin-4 by multidimensional heteronuclear magnetic-resonance spectroscopy. *Science*, **256**, 1673 (1992).
[16] A. Wlodawer, A. Pavlovsky, A. Gustchina. Crystal structure of human recombinant interleukin-4 at 2.25 Å resolution. *FEBS Lett.*, **309**, 59 (1992).
[17] M.R. Walter, W.J. Cook, B.G. Zhao, R.P. Cameron, S.E. Ealick, R.L. Walter, P. Reichert, T.L. Naganbushan, P.P. Trotta, C.E. Bugg. Crystal-structure of recombinant human interleukin-4. *J. Biol. Chem.*, **267**, 20371 (1992).
[18] T. Müller, F. Oehlenschlager, M. Buehner. Human interleukin-4 and variant R88Q: phasing X-ray diffraction data by molecular replacement using X-ray and nuclear-magnetic-resonance models. *J. Mol. Biol.*, **247**, 360 (1995).

[19] J.F. Bazan. Structural design and molecular evolution of a cytokine receptor super-family. *Proc. Natl. Acad. Sci. USA*, **87**, 6934 (1990).
[20] L.J. Smith, C. Redfield, R.A.G. Smith, C.M. Dobson, G.M. Clore, A.M. Gronenborn, M.R. Walter, T.L. Naganbushan, A. Wlodawer. Comparison of four independently determined structures of human recombinant interleukin-4. *Nat. Struct. Biol.*, **1**, 301 (1994).
[21] C. Redfield, J. Boyd, L.J. Smith, R.A.G. Smith, C.M. Dobson. Loop mobility in a four-helix-bundle protein: ^{15}N NMR relaxation measurements on human interleukin-4. *Biochemistry*, **31**, 10431 (1992).
[22] C. Redfield, R.A.G. Smith, C.M. Dobson. Structural characterization of a highly-ordered molten globule at low pH. *Nat. Struct. Biol.*, **1**, 23 (1994).
[23] A.E. Mark, W.F. van Gunsteren. Simulation of the thermal denaturation of hen egg-white lysozyme—trapping the molten globule state. *Biochemistry*, **31**, 7745 (1992).
[24] V. Dagget, M. Levitt. A model of the molten globule state from molecular-dynamics simulations. *Proc. Natl. Acad. Sci. USA*, **89**, 5142 (1992).
[25] L.J. Smith, C.M. Dobson, W.F. van Gunsteren. Molecular dynamics simulations of human α-lactalbumin: changes to the structural and dynamical properties of the protein at low pH. *Proteins*, **36**, 77 (1999).
[26] L.J. Smith, C.M. Dobson, W.F. van Gunsteren. Side-chain conformational disorder in a molten globule: molecular dynamics simulations of the A-state of human α-lactalbumin. *J. Mol. Biol.*, **286**, 1567 (1999).
[27] H. Fan, A.E. Mark. Relative stability of protein structures determined by X-ray crystallography or NMR-spectroscopy: a molecular dynamics simulation study. *Proteins*, **53**, 111 (2003).
[28] G.T. Ibragimova, R.C. Wade. Importance of explicit salt ions for protein stability in molecular dynamics simulation. *Biophys. J.*, **74**, 2906 (1998).
[29] M.A. Martí-Renom, J.M. Mas, B. Oliva, E. Querol, F.X. Avilés. Effects of counter-ions and volume on the simulated dynamics of solvated proteins. Application to the activation domain of procarboxypeptidase B. *Protein Eng.*, **11**, 881 (1998).
[30] S. Pfeiffer, D. Fushman, D. Cowburn. Impact of Cl^- and Na^+ ions on simulated structure and dynamics of beta ARK1 PH domain. *Proteins Struct. Funct. Genet.*, **35**, 206 (1999).
[31] P. Drabik, A. Liwo, C. Czaplewski, J. Ciarkowski. The investigation of the effects of counterions in protein dynamics simulations. *Protein Eng.*, **14**, 747 (2001).
[32] P.K. Weiner, P.A. Kollman. AMBER: assisted model building with energy refinement. A general program for modeling molecules and their interactions. *J. Comput. Chem.*, **2**, 287 (1981).
[33] W.D. Cornell, P. Cieplak, C.I. Bayly, I.R. Gould, K.M. Merz, D.M. Ferguson, D.C. Spellmeyer, T. Fox, J.W. Caldwell, P.A. Kollman. A 2nd generation force-field for the simulation of proteins, nucleic-acids and organic-molecules. *J. Am. Chem. Soc.*, **117**(19), 5179 (1995) May.
[34] D.A. Pearlman, D.A. Case, J.W. Caldwell, W.S. Ross, T.E. Cheatham III, S. DeBolt, D. Ferguson, G. Seibel, P.A. Kollman. AMBER, a package of computer programs for applying molecular mechanics, normal mode analysis, molecular dynamics and free energy calculations to simulate the structural and energetic properties of molecules. *Comput. Phys. Commun.*, **91**, 1 (1995).
[35] B.R. Brooks, R.E. Bruccoleri, B.D. Olafson, D.J. States, S. Swaminathan, M. Karplus. CHARMM: a program for macromolecular energy, minimization and dynamics calculations. *J. Comput. Chem.*, **4**, 187 (1983).
[36] A.D. MacKerell Jr., J. Wirkiewicz-Kuczera, M. Karplus. An all-atom empirical energy function for the simulation of nucleic acids. *J. Am. Chem. Soc.*, **117**, 11946 (1975).
[37] A.D. MacKerell, D. Bashford, M. Bellott, R.L. Dunbrack, J.D. Evanseck, M.J. Field, S. Fischer, J. Gao, H. Guo, S. Ha, D. Joseph-McCarthy, L. Kuchnir, K. Kuczera, F.T.K. Lau, C. Mattos, S. Michnick, T. Ngo, D.T. Nguyen, B. Prodhom, W.E. Reiher, B. Roux, M. Schlenkrich, J.C. Smith, R. Stote, J. Straub, M. Watanabe, J. Wiórkiewicz-Kuczera, D. Yin, M. Karplus. All-atom empirical potential for molecular modeling and dynamics studies of proteins. *J. Phys. Chem. B*, **102**, 3586 (1998).
[38] W.L. Jorgensen, J. Tirado-Rives. The OPLS potential functions for proteins, energy minimizations for crystals of cyclic peptides and crambin. *J. Am. Chem. Soc.*, **110**, 1657 (1988).
[39] W.L. Jorgensen, D.S. Maxwell, J. Tirado-Rives. Development and testing of the OPLS all-atom force field on conformational energetics and properties of organic liquids. *J. Am. Chem. Soc.*, **118**, 11225 (1996).
[40] W.F. van Gunsteren, H.J.C. Berendsen. *Groningen Molecular Simulation (GROMOS) Library Manual*, BIOMOS, Groningen (1987).
[41] W.F. van Gunsteren, S.R. Billeter, A.A. Eising, P.H. Hünenberger, P. Krüger, A.E. Mark, W.R.P. Scott, I.G. Tironi. *Biomolecular Simulation: The GROMOS96 Manual and User Guide*, Verlag der Fachvereine, Zürich (1996).
[42] L.D. Schuler, X. Daura, W.F. van Gunsteren. An improved GROMOS96 force field for aliphatic hydrocarbons in the condensed phase. *J. Comput. Chem.*, **22**, 1205 (2001).
[43] A. Villa, A.E. Mark. Calculation of the free energy of solvation for neutral analogs of amino acid side chains. *J. Comput. Chem.*, **23**, 548 (2002).
[44] J.L. MacCallum, D.P. Tieleman. Calculation of the water-cyclohexane transfer free energies of neutral amino acid side-chain analogs using the OPLS all-atom force field. *J. Comput. Chem.*, **24**, 1930 (2003).
[45] M.R. Shirts, J.W. Pitera, W.C. Swope, V.S. Pande. Extremely precise free energy calculations of amino acid side chain analogs: comparison of common molecular mechanics force fields for proteins. *J. Chem. Phys.*, **119**, 5740 (2003).
[46] C. Oostenbrink, A. Villa, A.E. Mark, W.F. van Gunsteren. A biomolecular force field based on the free enthalpy of hydration and solvation: the *GROMOS* force-field parameter sets 53A5 and 53A6. *J. Comput. Chem.*, **25**, 1656 (2004).
[47] W.R.P. Scott, P.H. Hünenberger, I.G. Tironi, A.E. Mark, S.R. Billeter, J. Fennen, A.E. Torda, T. Huber, P. Krüger, W.F. van Gunsteren. The *GROMOS* biomolecular simulation program package. *J. Phys. Chem. A*, **103**, 3596 (1999).
[48] H.J.C. Berendsen, J.P.M. Postma, W.F. van Gunsteren, J. Hermans. Interaction models for water in relation to protein hydration. In *Intermolecular Forces*, B. Pullman (Ed.), pp. 331–342, Reidel, Dordrecht (1981).
[49] J.P. Ryckaert, G. Ciccotti, H.J.C. Berendsen. Numerical integration of the cartesian equations of motion of a system with constraints: molecular dynamics of *n*-alkanes. *J. Comput. Phys.*, **23**, 327 (1977).
[50] I.G. Tironi, R. Sperb, P.E. Smith, W.F. van Gunsteren. A generalized reaction field method for molecular dynamics simulations. *J. Chem. Phys.*, **102**, 5451 (1995).
[51] A. Glättli, X. Daura, W.F. van Gunsteren. Derivation of an improved simple point charge model for liquid water: SPC/A and SPC/L. *J. Chem. Phys.*, **116**, 9811 (2002).
[52] H.J.C. Berendsen, J.P.M. Postma, W.F. van Gunsteren, A. DiNola, J.R. Haak. Molecular dynamics with coupling to an external bath. *J. Chem. Phys.*, **81**, 3684 (1984).
[53] B.A. Luty, W.F. van Gunsteren. Calculating electrostatic interactions using the particle–particle particle–mesh method with nonperiodic long-range interactions. *J. Phys. Chem.*, **100**, 2581 (1996).
[54] I.G. Tironi, B.A. Luty, W.F. van Gunsteren. Space-time correlated reaction field: a stochastic dynamical approach to the dielectric continuum. *J. Chem. Phys.*, **106**, 6068 (1997).
[55] P.H. Hünenberger, J.A. McCammon. Ewald artifacts in computer simulations of ionic solvation and ion–ion interaction: a continuum electrostatics study. *J. Chem. Phys.*, **110**, 1856 (1999).
[56] P.H. Hünenberger, J.A. McCammon. Effect of artificial periodicity in simulations of biomolecules under Ewald boundary conditions: a continuum electrostatics study. *Biophys. Chem.*, **78**, 69 (1999).
[57] W. Weber, P.H. Hünenberger, J.A. McCammon. Molecular dynamics simulations of a polyalanine octapeptide under Ewald boundary conditions: influence of artificial periodicity on peptide conformation. *J. Phys. Chem. B*, **104**, 3668 (2000).
[58] T.M. Nymand, P. Linse. Ewald summation and reactions field methods for potentials with atomic charges, dipoles, and polarizabilities. *J. Chem. Phys.*, **112**, 6152 (2000).
[59] R. Walser, P.H. Hünenberger, W.F. van Gunsteren. Comparison of different schemes to treat long-range electrostatic interactions in molecular dynamics simulations of a protein crystal. *Proteins*, **43**, 509 (2001).
[60] R. Kaptein, E.R.P. Zuiderweg, R.M. Scheek, R. Boelens, W.F. van Gunsteren. A protein structure from nuclear magnetic resonance data: *lac* repressor headpiece. *J. Mol. Biol.*, **182**, 179 (1985).
[61] W.F. van Gunsteren, R. Boelens, R. Kaptein, R.M. Scheek, E.R.P. Zuiderweg. *An Improved Restrained Molecular Dynamics Technique to Obtain Protein Tertiary Structure from Nuclear Magnetic*

Resonance Data. Polycrystal Book Service, P. O. Box 27, 60558 Western Springs, ILL (1985).

[62] K. Wüthrich, M. Billeter, W. Braun. Pseudo-structures for the 20 common amino-acids for use in studies of protein conformations by measurements of intramolecular proton proton distance constraints with nuclear magnetic-resonance. *J. Mol. Biol.*, **169**, 949 (1983).

[63] M. Christen, P. Hünenberger, D. Bakowies, R. Baron, R. Bürgi, D.P. Geerke, T.N. Heinz, M.A. Kastenholz, V. Kräutler, C. Oostenbrink, C. Peter, D. Trzesniak, W.F. van Gunsteren. The GROMOS software for biomolecular simulation: GROMOS05. *J. Comput. Chem.*, **26**, 1719 (2005).

[64] V. Kräutler, M. Kastenholz, P.H. Hünenberger. The esra molecular mechanics analysis package. available at http://esra.sf.net (2005).

[65] W. Kabsch, C. Sander. Dictionary of protein secondary structure—pattern-recognition of hydrogen-bonded and geometrical features. *Biopolymers*, **22**, 2577 (1983).

[66] J. Tropp. Dipolar relaxation and nuclear Overhauser effects in nonrigid molecules: the effect of fluctuating internuclear distances. *J. Chem. Phys.*, **72**, 6035 (1980).

[67] M. Karplus. Contact electron-spin coupling of nuclear magnetic moments. *J. Chem. Phys.*, **30**, 11 (1959).

[68] G.W. Vuister, A. Bax. Quantitative *J* correlation: a new approach for measuring homonuclear three-bond $J(H^N, H^\alpha)$ coupling-constants in ^{15}N-enriched proteins. *J. Am. Chem. Soc.*, **115**, 7772 (1993).

[69] E.R. Henry, A. Szabo. Influence of vibrational motion on solid-state line-shapes and NMR relaxation. *J. Chem. Phys.*, **82**, 4753 (1985).

[70] W.F. van Gunsteren, D. Bakowies, D. Damm, T. Hansson, U. Stocker, X. Daura. Practical aspects of simulation studies of biomolecular systems. In *NATO ASI Series A 315: Dynamics, Structure and Function of Biological Macromolecules*, O. Jardetzky, M.D. Finucane (Eds.), pp. 1–26, IOS Press, Amsterdam (2001).

[71] J. Evenäs, S. Forsén, A. Malmendal, M. Akke. Backbone dynamics and energetics of a calmodulin domain mutant exchanging between closed and open conformations. *J. Mol. Biol.*, **289**, 603 (1999).

[72] U. Stocker, K. Spiegel, W.F. van Gunsteren. On the similarity of properties in solution or in the crystalline state: a molecular dynamics study of hen lysozyme. *J. Biomol. NMR*, **18**, 1 (2000).

[73] H.B. Yu, M. Amann, T. Hansson, J. Köhler, G. Wich, W.F. van Gunsteren. Effect of methylation on the stability and solvation free energy of amylose and cellulose fragments: a molecular dynamics study. *Carbohydr. Res.*, **339**, 1697 (2004).

[74] T. Soares, X. Daura, C. Oostenbrink, L.J. Smith, W.F. van Gunsteren. Validation of the *GROMOS* force-field parameter set 45A3 against nuclear magnetic resonance data of hen egg lysozyme. *J. Biomol. NMR*, **30**, 407 (2004).

[75] M. Becke (Ed.). *Gmelin Handbuch der anorganischen Chemie*, 8th ed., Springer Verlag, Berlin (1974).

[76] P. Vanysek. Ionic conductivity and diffusion at infinite dilution. *CRC Handbook of Chemistry and Physics*, 79th ed., p. 86, CRC, Boca Raton, FL (2006).